

Structural, microstructural, and electrical properties of gold films and Schottky contacts on remote plasma-cleaned, *n*-type ZnO{0001} surfaces

Cite as: J. Appl. Phys. **97**, 103517 (2005); <https://doi.org/10.1063/1.1898436>

Submitted: 06 July 2004 • Accepted: 08 March 2005 • Published Online: 06 May 2005

B. J. Coppa, C. C. Fulton, S. M. Kiesel, et al.



View Online



Export Citation

ARTICLES YOU MAY BE INTERESTED IN

ZnO Schottky barriers and Ohmic contacts

Journal of Applied Physics **109**, 121301 (2011); <https://doi.org/10.1063/1.3581173>

A comprehensive review of ZnO materials and devices

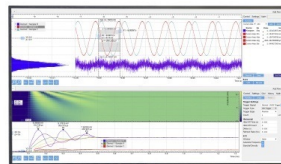
Journal of Applied Physics **98**, 041301 (2005); <https://doi.org/10.1063/1.1992666>

Gold Schottky contacts on oxygen plasma-treated, *n*-type ZnO(0001)

Applied Physics Letters **82**, 400 (2003); <https://doi.org/10.1063/1.1536264>

Challenge us.

What are your needs for
periodic signal detection?



Zurich
Instruments

Structural, microstructural, and electrical properties of gold films and Schottky contacts on remote plasma-cleaned, *n*-type ZnO{0001} surfaces

B. J. Coppa, C. C. Fulton, S. M. Kiesel, and R. F. Davis^{a)}

Department of Materials Science and Engineering, North Carolina State University, P.O. Box 7907, Raleigh, North Carolina 27695

C. Pandarinath, J. E. Burnette, and R. J. Nemanich

Department of Physics, North Carolina State University, P.O. Box 8202, Raleigh, North Carolina 27695

D. J. Smith

Department of Physics and Astronomy, Center for Solid State Science, Arizona State University, Tempe, Arizona 85287

(Received 6 July 2004; accepted 8 March 2005; published online 6 May 2005)

Current–voltage measurements of Au contacts deposited on *ex situ* cleaned, *n*-type ZnO(0001) [(000 $\bar{1}$)] surfaces showed reverse bias leakage current densities of ~ 0.01 (~ 0.1) A/cm² at 4.6 (3.75) V reverse bias and ideality factors >2 (both surfaces) before sharp, permanent breakdown (soft breakdown). This behavior was due primarily to the presence of $(1.6\text{--}2.0)\pm 0.1$ [(0.7–2.6) ± 0.1] monolayers (ML) of hydroxide, which forms an electron accumulation layer and increases the surface conductivity. *In situ* remote plasma cleaning of the (0001) [(000 $\bar{1}$)] surfaces using a 20 vol % O₂/80 vol % He mixture for the optimized temperatures, times, and pressure of 550 ± 20 °C (525 ± 20 °C), 60 (30) min, and 0.050 Torr reduced the thickness of the hydroxide layer to $\sim 0.4\pm 0.1$ ML and completely eliminated all detectable hydrocarbon contamination. Subsequent cooling of both surfaces in the plasma ambient resulted in the chemisorption of oxygen and a change from 0.2 eV of downward band bending for samples cooled in vacuum to 0.3 eV of upward band bending indicative of the formation of a depletion layer of lower surface conductivity. Cooling in either ambient produced stoichiometric ZnO{0001} surfaces having an ordered crystallography as well as a step-and-terrace microstructure on the (000 $\bar{1}$) surface; the (0001) surface was without distinctive features. Sequentially deposited, unpatterned Au films, and presumably the rectifying gold contacts, initially grew on both surfaces cooled in the plasma ambient via the formation of islands that subsequently coalesced, as indicated by calculations from x-ray photoelectron spectroscopy data and confirmed by transmission electron microscopy. Calculations from the current–voltage data of the best contacts revealed barrier heights on the (0001) [(000 $\bar{1}$)] surfaces of 0.71 ± 0.05 (0.60 ± 0.05) eV, a saturation current density of $(4\pm 0.5)\times 10^{-6}$ A/cm² ($2.0\pm 0.5\times 10^{-4}$ A/cm²), a lower value of $n=1.17\pm 0.05$ (1.03 ± 0.05), a significantly lower leakage current density of $\sim 1.0\times 10^{-4}$ A/cm² ($\sim 91\times 10^{-9}$ A/cm²) at 8.5 (7.0) V reverse bias prior to sharp, permanent breakdown (soft breakdown). All measured barrier heights were lower than the predicted Schottky–Mott value of 1.0 eV, indicating that the interface structure and the associated interface states affect the Schottky barrier. However, the constancy in the full width at half maximum of the core levels for Zn 2*p* (1.9 ± 0.1 eV) and O 1*s* (1.5 ± 0.1 eV), before and after sequential *in situ* Au depositions, indicated an abrupt, unreacted Au/ZnO(0001) interface. Transmission electron microscopy confirmed the abruptness of an epitaxial interface. Annealing the contacts on the (0001) surface to 80 ± 5 and 150 ± 5 °C resulted in decreases in the ideality factors to 1.12 ± 0.05 and 1.09 ± 0.05 and increases in saturation current density to 9.05 and 4.34 μ A/cm², the barrier height to 0.82 ± 0.5 and 0.79 ± 0.5 eV, and in the leakage current densities to $\sim 2\times 10^{-3}$ A/cm² at 6 V and $\sim 20\times 10^{-3}$ A/cm² at 7 V, respectively. © 2005 American Institute of Physics. [DOI: 10.1063/1.1898436]

I. INTRODUCTION

Zinc oxide (ZnO) occurs most commonly in the hexagonal wurtzite crystal structure that possesses a direct band gap of ~ 3.4 eV at room temperature and exhibits spontaneous polarization along the $\langle 0001 \rangle$ directions.¹ Reviews of the ba-

sic properties of this material and its use or potential use in selected applications have recently been published.^{1,2} Boules and wafers of ZnO are being produced commercially by several techniques. These materials are typically *n* type; this characteristic has traditionally been attributed to native defects such as oxygen vacancies and zinc interstitials.³ However, recent theoretical calculations by Kohan *et al.*⁴ have shown that none of the native defects exhibits characteristics

^{a)}Author to whom correspondence should be addressed; FAX: 919-515-7724; electronic mail: robert_davis@ncsu.edu

consistent with a high-concentration shallow donor. Van de Walle⁵ has noted that only vacancies have sufficiently low energies to form during the growth of ZnO; however, Zn and O vacancies act as deep acceptors and deep donors, respectively. First-principles calculations by the last author have provided evidence that H behaves as a shallow donor in ZnO and can be incorporated into the boule or thin film via the formation of O–H bonds at the surface during growth and as a component of the hydroxide that invariably forms on the surface of this crystal when exposed to the normal laboratory ambient. The determination in substrates produced commercially via vapor phase growth of (1) a very shallow donor energy level at ~ 37 meV via Hall measurements and (2) a donor-bound-exciton line (the 14 line) in photoluminescence studies at 5 K both of which disappear upon annealing in the range of 500–700 °C lends credence to this theory. On the contrary it has been argued⁶ that the primary role of H may be to passivate acceptors via the formation of complexes that bond with the acceptor species to produce a neutral charge state in each complex rather than residing only as compensating OH⁻ ions throughout the crystal. Hydrogen may also play both roles. However, electron-paramagnetic studies⁶ of ZnO substrates produced by all the commercial process routes employed at this writing have revealed sufficient concentrations of the shallow donor species of Al and, to a lesser extent Ga, to cause the *n*-type conductivity measured in these materials. Additional studies of the roles of all these species in producing the *n*-type conductivity are mandated; they must be removed or be significantly reduced ion concentration to allow controlled doping and to make repeatable the properties of optoelectronic and microelectronic devices produced from this material.

Several important ZnO-based devices employ Schottky barrier diodes (SBDs). For example, Schottky-type, ZnO ultraviolet photodetectors have technical advantages in speed and lower noise than their photoconductive counterpart.⁷ The former are expected to be particularly useful in space applications, as this material is very resistant to MeV proton irradiation relative to other semiconductors.⁸ These types of diodes are also essential for probing defects in semiconductors by junction spectroscopic characterization techniques such as deep-level transient spectroscopy⁹ (DLTS) and admittance spectroscopy.¹⁰ For example, Auret *et al.*⁹ employed Au as the rectifying contact on the O-polar ZnO(000 $\bar{1}$) surface for DLTS studies. They reported a 1-nA leakage current to an applied bias of -1 V and an ideality factor of 1.19.

The Schottky–Mott model¹¹ predicts that metals with high work functions are prime candidates for rectifying contacts on *n*-type semiconductors. In the case of ZnO, it has been shown¹² that these metals should also possess a low oxygen affinity; thus, the candidate materials of choice are essentially limited to gold, platinum, and palladium. Silver may also be a candidate metal; however, for long-term applications, it would have to be capped with a metal more resistant to oxidation. Kanai¹⁰ found that for gold contacts on as-received Si-polar Zn(0001) surfaces, electrons were possibly trapped at a surface state, which stretched out the capacitance–voltage (*C–V*) curve and decreased the capacitance at high frequencies. As an explanation of these charac-

teristics, this investigator inferred qualitatively that the likelihood of forming rectifying contacts on the ZnO(0001) surface may be limited by the polar and ionic character of this material. This character could lead to surface states that are occupied by free electrons that need not form ionic bonds with O atoms. In contrast, free electrons are not common on the polar ZnO(000 $\bar{1}$) face, reducing the likelihood of a surface state, which could lead to poor rectifying or ohmic behavior.

Only a few groups, at this writing, have reported investigations of Schottky contacts to ZnO. Neville and Mead¹³ employed *I–V*, *C–V*, photoresponse, and thermal activation energy measurements in an early study of the Schottky barrier height (Φ_B) for Au on chemically prepared ZnO crystals with an unspecified orientation. Their measurements resulted in a value of 0.66 eV. An ideality factor (*n*) of 1.05 was also reported [but below the valid forward bias (V_F) range of $V_F > 0.075$ V] without specifying the reverse bias leakage current. Fabricius *et al.*⁷ measured $n=2.7$ for Au Schottky photodiodes fabricated on as-received polycrystalline ZnO; however, neither the (Φ_B) nor the leakage currents were indicated. This high value of *n* was reportedly influenced by recombination processes. Rabadanov *et al.*¹² measured the same barrier height of 0.65 ± 0.05 eV for Au, Pt, Pd, and Ag contacts deposited in vacuum at room temperature on ZnO monocrystals of an unspecified orientation and cleaved in vacuum. However, neither the ideality parameters nor the breakdown voltages were reported. Ohashi *et al.*¹⁴ also deposited Au contacts on chemically prepared, O-polar (000 $\bar{1}$) surfaces of ZnO and obtained an ideality factor of 1.19 and reverse currents of 1 nA at 1 V. Silver Schottky contacts with a Au cap have been fabricated on as-received ZnO(11 $\bar{2}0$) epilayers.^{15,16} The values of Φ_B determined via *I–V* and *C–V* measurements, were 0.89 and 0.92 eV, respectively. A leakage current of 0.1 nA at 1-V reverse bias^{15,16} and an ideality factor of 1.33 (Ref. 16) were also reported. The high ideality factor was attributed to an interfacial layer and/or surface states. Polyakov *et al.*¹⁷ deposited both Au and Ag contacts to polished *n*-ZnO(0001) surfaces that were either exposed to organic solvents or etched in concentrated HCl or exposed to organic solvents and etched in concentrated HNO₃. They reported values of Φ_B determined using *C–V* measurements for both metals of 0.65–0.70 eV; these values are in good agreement with the values measured on gold contacts by other investigators (see above) and with the values obtained via *I–V* measurements in the present research on plasma-cleaned substrates. The saturation current densities ranged from 10^{-5} A/cm² on surfaces etched in HCl to 8×10^{-7} A/cm² on solvent-cleaned samples. The diode ideality factors ranged from 1.6 to 1.8 regardless of the treatment of the surface prior to the deposition of the contacts. More recently, electron-beam-induced current (EBIC) studies of the lateral homogeneity of Pd and Ag Schottky contacts on (0001) and (11 $\bar{2}0$) surfaces of ZnO films and of Pd, Au, Ag, and Ni contacts on the (0001) and the (000 $\bar{1}$) surfaces of ZnO wafers have been conducted by von Wenckstern *et al.*¹⁸ The films and wafers were exposed separately to various wet chemistries for cleaning and etching and to a N₂O plasma.

The EBIC studies revealed that the contacts deposited on the plasma-treated surfaces were homogeneous; whereas, the image of the contacts on the etched surfaces showed a veined structure that produced a very inhomogeneous contact. However, this veined microstructure did not correlate with the etch pits in the surfaces; thus, other reasons for the lateral variation of the induced current must be investigated. The effective barrier heights and ideality factors for the contacts ranged from 0.56 to 0.73 eV and 1.4 to 2.0 eV, respectively.

Device-quality Schottky contacts typically require intimate metal-semiconductor interfaces free of surface contamination. A major deterrent to the development of low leakage Schottky contacts on ZnO with low ideality parameters is the ~ 3 -monolayer- (ML) thick native contamination layer, which includes ~ 1 ML of adventitious carbon and ~ 2 ML of the aforementioned hydroxide.¹⁹ It has been proposed²⁰ that H atoms donate $\sim 0.5 e^-$ to each surface oxygen ion on both the (0001)- and (000 $\bar{1}$)-hydroxylated surfaces of ZnO. This strong interaction, comparable to O-metal bonding in the bulk oxide lattice, can result in the formation of a shallow electron donor state through the proposed reaction: ($H + O^{2-} \rightarrow OH^- + e^-$) and can increase the carrier concentration in the space-charge layer by several orders of magnitude.²⁰ As such, several groups^{21–23} have reported that the hydroxide leads to the formation of an accumulation layer that results in a high surface conductivity on both polar faces of ZnO. This is very likely the reason for the reported high leakage currents above -1 V (Refs. 8, 9, 12, 15, and 16) and relatively high ideality factors (>2) for high work-function metals (e.g., Au) deposited on these unclean surfaces. Moreover, the presence of these contaminants may introduce the interface states and the barrier for tunneling that are commonly used for explaining the high ideality factors.¹⁷

The sensitivity of the surface conductivity of ZnO to hydrogen and oxygen has been utilized in sensor devices.¹² In contrast with H, adsorbed oxygen species on ZnO act as electron acceptors that generate a depletion layer, which lowers the surface conductivity by several orders of magnitude^{24,25} and is advantageous for Schottky barrier formation. It has been proposed²⁶ that chemisorption of oxygen occurs preferentially at surface defect sites as O^{2-} or O^- .

In this study, an *in situ* remote plasma cleaning procedure and a subsequent oxidation step were developed in conjunction with the investigations of the deposition and the temperature-dependent current–voltage (I – V – T) properties of Au Schottky contacts on polished ZnO(0001) and ZnO(000 $\bar{1}$) surfaces. Photoemission of the electronic structure and the growth mode of the Au on the ZnO{0001} surfaces were also studied via x-ray photoelectron spectroscopy (XPS) and ultraviolet photoelectron spectroscopy (UPS). The structural and microstructural characteristics of all the materials used in this program were investigated using x-ray diffraction (XRD), low-energy electron diffraction (LEED), atomic force microscopy (AFM), and transmission electron microscopy (TEM).

II. EXPERIMENTAL PROCEDURES

Two-millimeter-thick, 2-in.-diameter ZnO(0001) and ZnO(000 $\bar{1}$) wafers, diced from boules, produced by seeded

chemical vapor transport by Eagle–Picher Technologies, Inc., and chemomechanically polished on both sides, were employed in the present research. Each wafer contained highly textured domains separated by low angle boundaries and with a collective range of full width at half maxima in their rocking curves acquired about the [0001] direction. A grade-I wafer, free of microvoids on the surface and internally, was used for the I – V – T studies. Grade-II wafers containing microvoids were used in all other experiments. The wafers were cleaved into smaller sections (>1 cm²), rinsed *ex situ* in methanol for 5 s, and dried in flowing nitrogen. Hall (van der Pauw configuration) and C – V measurements, the latter at 1×10^4 Hz, taken from the (0001) surface of both grades of *ex situ* cleaned wafers, showed a bulk carrier concentration of $(1 \pm 5) \times 10^{17}/\text{cm}^3$ and a nominal effective donor concentration, ($N_D - N_A$), of $(5 \pm 5) \times 10^{16}/\text{cm}^3$, respectively. It is important to note that all wafers were cleaned *ex situ* in the manner just noted prior to loading into UHV for *in situ* cleaning and the deposition of Au films and Schottky contacts, unless indicated otherwise. These samples are referred to as either the “*ex situ* cleaned” or the “as-loaded” samples in the following sections.

All *in situ* metal deposition, cleaning, and surface characterization experiments described below were conducted within a unique ultrahigh vacuum (UHV) configuration, which integrates several independent cleaning, thin-film growth, and analysis systems via a transfer line having a base pressure of $<1 \times 10^{-9}$ Torr.²⁷ A (40–100)-nm-thick Ti film was deposited by e-beam evaporation from a 99.999% pure metal source onto the entire (0001) or (000 $\bar{1}$) face of each ZnO section. This film served (1) to absorb radiation from the underlying Pt–Rh heater and to conduct heat into the wafer during the *in situ* cleaning of the opposite face and (2) as an ohmic contact. ZnO{0001} surfaces and Au/ZnO{0001} interfaces without detectable concentrations of hydrocarbons and with significantly reduced concentrations of hydroxide were achieved via exposure of the former to a 20-W, 20% O₂/80% He (by volume) remote plasma at either 525 ± 20 °C [(000 $\bar{1}$) surface] or at 550 ± 20 °C [(0001) surface] and 0.050 ± 0.001 Torr for either 30 min [(000 $\bar{1}$) surface] or 60 min. [(0001) surface]. Each cleaned surface was then cooled to either 425 °C and subsequently in vacuum or to room temperature in the unignited plasma gas. A detailed description of this cleaning procedure has been reported.²⁸

Gold was deposited *in situ* via e-beam evaporation from a 99.999% pure metal source onto the cleaned surfaces, cooled in the plasma gas ambient either sequentially as very thin films of increasing thickness or through a gold-coated molybdenum shadow mask as contacts having a nominal diameter and thickness of 100 μm and ~ 150 nm, respectively, and arranged in an 8×8 array. The diameters of laser-drilled holes in the shadow mask were not precisely 100 μm ; the areas calculated from the optically measured diameters of the contacts used in the electrical measurements are given where relevant in the following sections. The nominal thickness of each Au layer was determined using a quartz-crystal deposition rate monitor. The base and process pressures within the

3-kW Thermionics e-beam system, used to deposit both the Ti and the Au contacts, were $\sim 7 \times 10^{-10}$ and $\sim 7 \times 10^{-9}$ Torr, respectively. Deposition rates varied from 0.1–1 Å/s, depending on the application, and were regulated with a Sycon Instruments STM-100 MF film thickness/rate monitor. The resulting Au/ZnO/Ti structure allowed current to pass through the bulk wafer and eliminated the need for complex isolation of the contacts.

Current–voltage results were acquired for all samples at either room temperature or an elevated temperature using 50- μm -diameter tungsten fine-wire-tip probes and a Keithley 236 source unit having the capability of measuring currents in the 1 pA–100 mA range. Selected samples were heated on the sample stage to 80 ± 5 and 150 ± 5 °C for subsequent temperature-dependent analyses. A hand-held K-type thermocouple in contact with the Au surface provided digital temperature readout. C–V measurements were used for determining the series resistance of the wafers and were performed using a Hewlett–Packard LCR meter with the capability of measuring capacitances in the range (0.01 fF–10 μF).

XRD 2θ scans were conducted *ex situ* on an unannealed and annealed 100-nm-thick Au films to determine their crystallographic orientation and stability during heating. A Rigaku Geigerflex diffractometer was used with Cu $K\alpha$ ($\lambda = 0.1542$ nm) radiation at a tube voltage and current of 27 kV and 20 mA, respectively. The x-ray beam was directed by 1° diffraction and scattering slits to a scintillator detector having a resolution of 43%.

Transmission electron microscopy was used to characterize the interface between the ~ 100 -nm-thick Au layer, used in the XRD studies and deposited in the same manner as the contacts, and a ZnO(000 $\bar{1}$) substrate. Cross sections of unannealed and annealed (150 ± 5 °C, 15 min) samples were prepared by sandwiching two ZnO pieces, each having the dimensions of $\sim 0.1 \times 0.3$ cm², between two sapphire support pieces of the same size using M-Bond epoxy. The epoxy was cured at 120 °C for 2 h. The sandwich was then flattened on one side using a 15- μm diamond disk and dimpled to a depth of 30–35 μm with 6- μm diamond paste and 10 g of weight on the sample holder. The sample was subsequently polished on a felt wheel embedded with 1- μm diamond paste with a weight of 20 g to eliminate as many scratches as possible. The four corners surrounding the dimple were flattened with 6- μm diamond paper.

The sample was then inverted onto a glass peg with wax and polished using 9-, 6-, 3-, and 1- μm diamond papers to a thickness of 30–50 μm , as determined using the colors of the Nomarski fringes for ZnO shown in Table 3.1 in Ref. 29. A copper ring was glued onto the flat, polished side of the sample using M-bond. Ion milling at angles of 17° (unannealed) or 13° (annealed) using Ar⁺ ions generated using a gun voltage of 4 keV (unannealed) or 3 keV (annealed) was used as the final thinning step. The samples were cooled by a liquid-nitrogen stage to reduce the damage caused by the impinging ion beam.

The TEM samples were analyzed using bright-field imaging, selected area electron diffraction (SAED), and high-resolution transmission electron microscopy (HRTEM) im-

aging in a JEOL JEM4000EX TEM operating at 400 kV. An objective aperture was employed to filter out the inelastically scattered electrons and thereby enhance the contrast.

III. RESULTS AND DISCUSSION

A. Analyses of the plasma-cleaned ZnO{0001} surfaces cooled in vacuum

Extensive XPS, UPS, and LEED investigations concerned with the hydroxide and hydrocarbon contamination on *ex situ* cleaned (as-loaded) {0001} surfaces of ZnO wafers and the removal of this chemistry via exposure to an oxygen/helium plasma at elevated temperatures accompanied by subsequent cooling to room temperature in vacuum have recently been conducted in the authors' laboratories. This subsection gives a succinct review and additional comments concerning the published results of this research²⁸ to provide to the reader the necessary information to understand the results of the present study. Section III B introduces related, unpublished results of subsequent cleaning studies pertinent to the present study wherein the cleaned ZnO{0001} samples were cooled to room temperature in the plasma ambient rather in vacuum.

Deconvolution of the O 1s core-level peak obtained via XPS studies of both the as-loaded (0001) and (000 $\bar{1}$) surfaces revealed two peaks at 530.9 and 532.9 eV indicative of O–Zn and O–OH bonding, respectively, as shown in spectrum (i) for the (0001) surface in Fig. 1(a). The position of this peak was the same within experimental error (± 0.1 eV) for the (000 $\bar{1}$) surface. Determination of the area under the peak at 532.9 eV for the ZnO(0001) samples showed that this surface contained $(1.6\text{--}2.0) \pm 0.1$ ML [(16–20) ± 1 at % of the measured volume] of OH with the average of three samples being 1.9 ML. Similar experiments conducted on the ZnO(000 $\bar{1}$) samples showed that this surface contained $(0.7\text{--}2.6) \pm 0.1$ ML [(7–26) ± 1 at % of the measured volume] of OH with the average of 14 samples being 1.5 ML. Analogous calculations using the C 1s peak revealed approximately 1 ML of adventitious carbon on both surfaces.

The remote plasma cleaning process reduced the concentrations of carbon species on both surfaces to below the detection limit of our XPS of 0.3 at. %. Examination of the XPS spectra of the (0001) surface cleaned in the plasma under the optimum conditions of 550 °C, 0.050 Torr, and 60 min revealed a shift in the lattice O 1s peak from 530.9 [full width half maximum (FWHM)=1.6 eV] to 530.4 eV (FWHM=1.4 eV), as shown in spectrum (ii) in Fig. 1(a). Similar studies concerning the XPS spectra of the (000 $\bar{1}$) surface cleaned in the plasma under the optimum conditions of 525 °C, 0.050 Torr, and 30 min revealed the same shift in the lattice O 1s peak with the peak having the same FWHM. These shifts in the O 1s peak for both orientations are attributed to a change in band bending (see UPS results below). The spectra acquired from the cleaned (0001) and (000 $\bar{1}$) surfaces also showed a peak at 532.7 and 532.4 eV, respectively, the areas of which were indicative of ~ 0.4 ML of residual OH on the surface. A corresponding core-level shift of 0.6 eV was deduced from the changes in the respective Zn

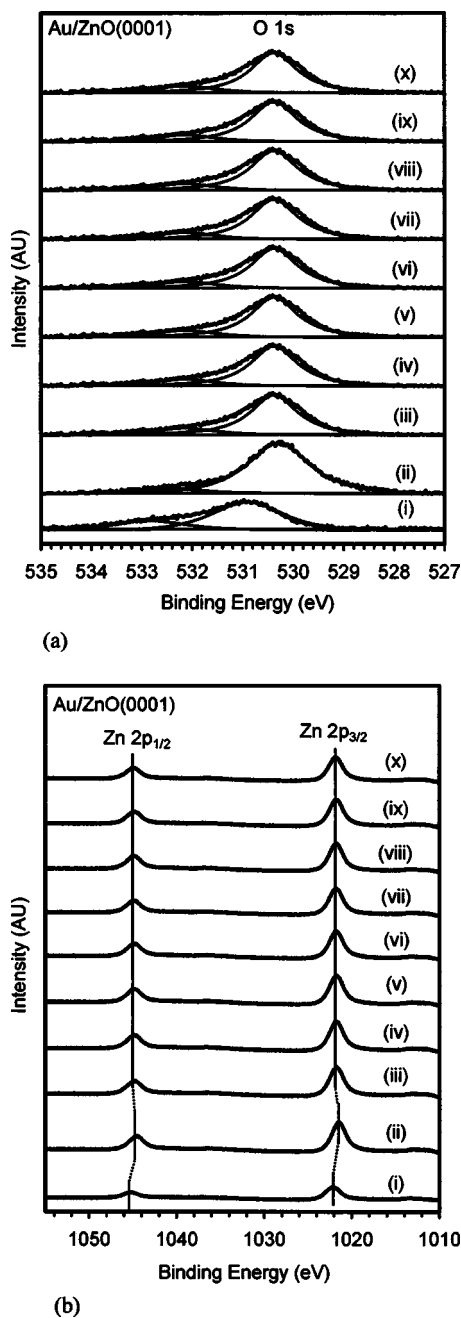


FIG. 1. (a) XPS O 1s core-level spectra acquired from the ZnO(0001) surface and (b) XPS Zn 2p_{1/2} and Zn 2p_{3/2} core-level spectra acquired from the ZnO(0001) surface under the conditions of (i) as-loaded, (ii) after remote plasma cleaning and cooling in either a vacuum or the plasma ambient (identical spectra were obtained), and after sequential depositions of (iii) 0.2, (iv) 0.4, (v) 0.6, (vi) 1.1, (vii) 1.3, (viii) 1.7, (ix) 2.2, and (x) 5.0 nm of a Au film. All spectra were acquired using Mg K α ($h\nu=1253.6$ eV) radiation.

2p_{3/2} and Zn 2p_{1/2} peak positions from 1022.0 and 1045.1 eV (both FWHM=2.0 eV) for the as-loaded samples to 1021.4 and 1044.5 eV (both FWHM=2.1 eV) after plasma cleaning, as shown in spectra (i) and (ii) for the (0001) surface in Fig. 1(b). The same shifts were observed in these spectra acquired from the (0001) surface. These shifts are also attributed to a change in band bending. The positions of all the XPS peaks noted above had an uncertainty of ± 0.1 eV. The Zn/O ratio increased from the range of 0.2–0.4 for the as-loaded samples to 1.0 for the plasma-cleaned samples.

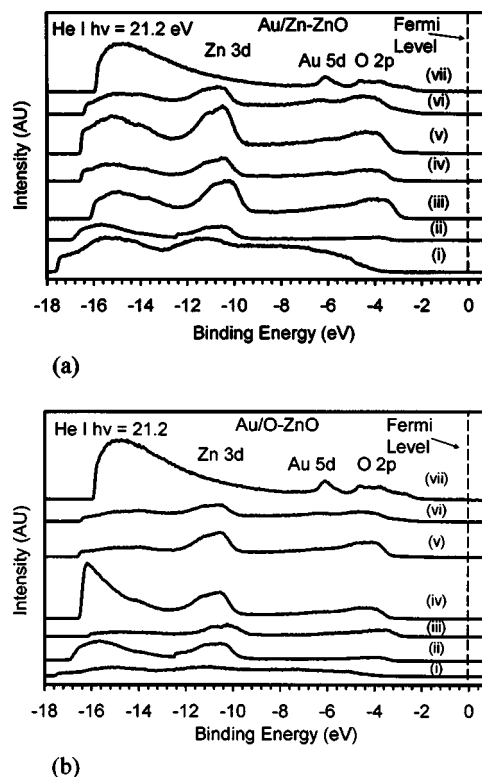


FIG. 2. UPS valence-band spectra acquired from the (a) (0001) surface and (b) the (0001) surface under the conditions (i) as-loaded, (ii) after exposure to a 20-W 20% O₂/80% He remote plasma and cooling in vacuum, (iii) after exposure to a 20-W 20% O₂/80% He remote plasma and cooling in the unignited plasma ambient, and after sequential depositions of Au to thicknesses of (iv) 0.2, (v) 0.4, (vi) 5.0, and (vii) 100 nm. Au-induced band bending is indicated by the shifts in the peak positions of the Zn 3d and O 2p bulk features between spectrums (iii) and (iv). All spectra were acquired using the He I photon line ($h\nu=21.2$ eV). The binding energy is measured with respect to the Fermi level ($E_F=0$ eV).

The removal of the OH to ~ 0.4 ML using the optimum cleaning conditions was critical for markedly reducing the proposed accumulation layer of high surface conductivity^{21–23} and for generating a surface with a Zn/O stoichiometric ratio of 1.0. Spectrum (i) acquired via UPS studies and shown in Figs. 2(a) and 2(b) for the (0001) the (0001) surfaces, respectively, reveals that the Zn 3d bulk feature for both as-loaded surfaces was located at 11.3 eV below the Fermi level, while the O 2p bulk feature was not discernable. Spectrum (ii) in these figures reveals that after plasma cleaning the O 2p feature begin to emerge at 4.0 eV, and a 0.6-eV shift occurred in the Zn 3d bulk feature to 10.7 eV that matched the corresponding change in band bending determined from the XPS spectra for the Zn 2p multiplet. The associated changes in band bending for both surfaces were also confirmed and determined quantitatively from these respective UPS spectra (± 0.1 -eV uncertainty). The bulk Fermi level in ZnO is accepted to be 0.3 eV below the conduction-band minimum³⁰ (CBM), and this value was also used in determining the band bending. The electronic band structures shown in Fig. 3, derived from spectra (i), (ii), and (iii) shown in Figs. 2(a) and 2(b), were identical for both surfaces. Figures 3(a) and 3(b) show that (i) the surface Fermi level shifted from 0.6 eV above the CBM for the

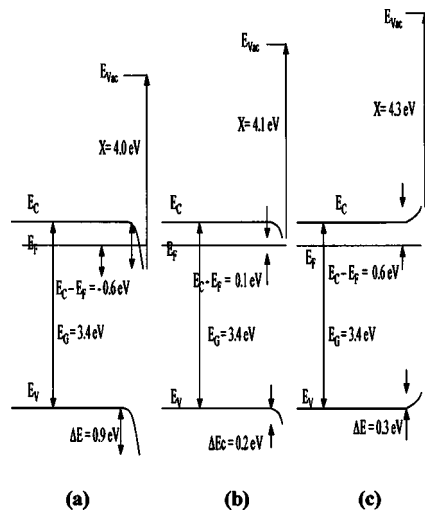


FIG. 3. Electronic band structure derived from UPS spectra for ZnO{0001} surfaces (a) in the as-loaded state, (b) after exposure to a 20-W 20% O₂/80% He remote plasma and cooling in vacuum, and (c) after exposure to the remote plasma and cooling in the unignited plasma ambient to room temperature.

as-loaded ZnO(0001) to 0.1 eV below the CBM after plasma cleaning and cooling in vacuum and (ii) the downward band bending was reduced from 0.9 to 0.2 eV as a result of using this same procedure because of the reduction in the aforementioned accumulation layer. The electron affinity of 4.0 ± 0.2 eV, also derived from the UPS spectra, essentially remained constant after cleaning.

B. Analyses of the plasma-cleaned ZnO{0001} surfaces cooled in the plasma ambient

It was subsequently determined from electrical measurements that cooling the cleaned {0001}-oriented samples in the O₂-containing, unignited plasma gas from 550 °C to room temperature improved the behavior of the subsequently deposited contacts. Investigations of Henrich and Cox³¹ showed that changes in the electron energy loss (EELS) and the UPS spectra occur upon chemisorption of O₂ on ZnO. The actual coverage of the surface was determined³¹ to be $< 2.5 \times 10^{-4}$ ML in the chemisorption temperature range (20–377 °C) with a sticking coefficient of 10^{-5} . These studies also revealed that more O₂ is adsorbed on the (000 $\bar{1}$) face than on a similarly prepared (0001) face; this may be associated with the preferential adsorption of oxygen to the atomic steps observed by the present authors on the former surface but not on the latter surface only after plasma cleaning.²⁸ Typically, the chemisorbed O₂ resides on the surface as O₂⁻, although it has been found as O⁻ as well.^{25,31} Physisorption of O₂ primarily occurs below 20 °C without any detectable charge transfer.³¹ However, O₂ that adsorbs to the surface has been shown to change the band bending by ~ 1 eV, consequently decreasing the surface conductivity by several orders of magnitude.²⁵ Analyses of the associated XPS spectra acquired in our studies indicated no change in either the O or the Zn core-level positions or the value of 1.0 for the Zn/O ratio previously determined for these surfaces cooled in vacuum. However, variations were observed in the

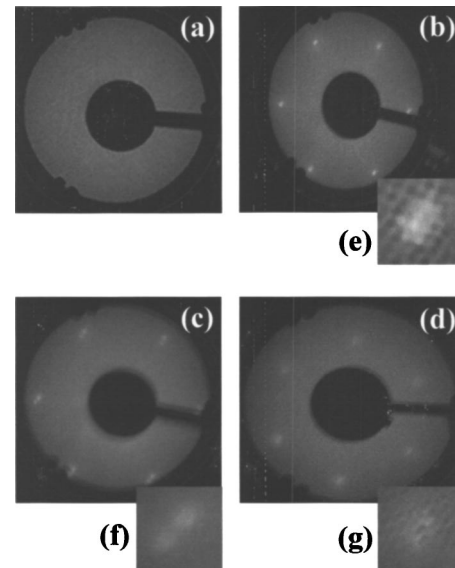


FIG. 4. LEED images and insets of a more highly magnified spot within these images of ZnO(000 $\bar{1}$) surfaces at primary beam energies of (a) 100 eV for samples in the as-loaded state (b) 42 eV after remote plasma cleaning and cooling in vacuum, (c) 42 eV after remote plasma cleaning and cooling in the plasma ambient, and (d) 80 eV after 100 nm of Au had been sequentially deposited.

spectra acquired from the more surface-sensitive UPS studies relative to the spectra for the cleaned samples cooled in vacuum and which subsequently matched the depletion layer model²⁵ shown in Fig. 3, as described below.

The UPS results provided evidence for a change in band bending that is associated with O₂ adsorption and that is preferable for the formation of a Schottky barrier with a material having a high work function such as Au. Figures 3(b) and 3(c) show that the 0.2 eV of downward band bending for the {0001} surfaces cooled in vacuum is changed to 0.3 eV of upward band bending due to the exposure of these cleaned surfaces to the unignited, O₂-containing plasma gas during cooling. This corresponds to a shift of the Zn 3d feature from 10.7 eV for the plasma-cleaned surfaces cooled in vacuum to 10.4 eV for the samples cooled in the O₂/He ambient. Figures 3(b) and 3(c) also indicate that the surface Fermi level shifted from 0.1 eV below the CBM for cleaned ZnO{0001} surfaces cooled in vacuum to 0.6 eV below the CBM for surfaces cooled in the O₂-containing gas. This shift away from the CBM corresponds to a reduction in *n*-type surface conductivity and may be attributed to the adsorption of oxygen species that act as electron acceptors in ZnO.²⁵ The electron affinity also varied from $(4.1-4.3) \pm 0.2$ eV between the two processing steps. Surface states were not observed after cooling in either vacuum or the plasma ambient.²⁸

Low-energy electron diffraction at a primary beam energy of 100 eV of the {0001} surfaces of the as-loaded ZnO samples exhibited only a bright background, as shown in the representative Fig. 4(a), that is indicative of a disordered contamination layer.²⁰ A (1 × 1) hexagonal LEED pattern containing slightly broadened spots was acquired from the (000 $\bar{1}$) surface at 42 eV in the plasma-cleaned sample cooled in vacuum, as shown in Fig. 4(b) and its associated inset of a more highly magnified spot. A similar pattern with distinctly

separated spots was acquired at the same voltage from the (0001) surface of similarly cleaned samples cooled in the plasma ambient, as shown in Fig. 4(c) and its inset. These separated spots were a function of the surface or very near surface structure, as LEED patterns acquired using beams having energies of 50 and 60 eV which penetrated more deeply the cleaned ZnO(0001) surfaces cooled in vacuum and in the plasma ambient, respectively, showed only distinct, unbroadened spots.

Prior and postcleaning AFM analysis of the microstructures of the (0001) surface and the (000 $\bar{1}$) surface confirmed the absence of any observable damage associated with the annealing and/or the plasma exposure.²⁸ The rms surface roughness values of the former and the latter surfaces were 1.2 ± 0.2 and 0.2 ± 0.2 nm before and 1.7 ± 0.2 and 0.6 ± 0.2 nm after cleaning, respectively. Highly ordered atomic steps with a unit-cell step height of 0.53 ± 0.05 nm and step width of ~ 0.2 μm were observed only on the (000 $\bar{1}$) surface.²⁸

C. Growth mode of Au films

The growth mechanism of Au deposited on the cleaned (0001) surface exposed to the plasma ambient on cooling was determined from the attenuation of the O 1s core levels as a function of increasing thickness of a sequentially deposited Au layer and shown in XPS spectra (iii)–(x) in Fig. 1(a) using an approach employed by Sitar *et al.*³² and Wolter *et al.*³³ The three possible growth modes considered in this study were (i) Frank–van der Merwe (two-dimensional, layer-by-layer growth), (ii) Volmer–Weber (three-dimensional growth of discrete islands), and (iii) Stranski–Krastanov (a combination of the two previous models wherein the initial film growth occurs via a layer-by-layer mechanism and is subsequently followed by the initiation of island growth). In these models, the surface energies of the substrate and the film and the interfacial energy and stress that result when these two material entities are joined determine the prevailing growth mode.

In XPS measurements, Frank–van der Merwe (FM) growth is expressed as

$$I_s/I_o = \exp(-t/\lambda_o), \quad (1)$$

where I_s is the core-level intensity for a given overlayer thickness (t), I_o is the baseline core-level intensity acquired from the ZnO surface following the cleaning and subsequent O₂ exposure, and λ_o is the attenuation length of the particular core-level electron. A Volmer–Weber (VW) mode of deposition would follow the expression

$$I_s/I_o = (1 - \theta) + \theta \exp(-t/\lambda_o), \quad (2)$$

where θ is the surface coverage of the islands (a value between 0 and 1). Stranski–Krastanov (SK) growth is represented by the expression

$$I_s/I_o = (1 - \theta) \exp(-q/\lambda_o) + \theta \exp(-t/\lambda_o), \quad (3)$$

where q is the deposited thickness before three-dimensional island growth or nucleation. The graphs of these three equations are shown in Fig. 5.

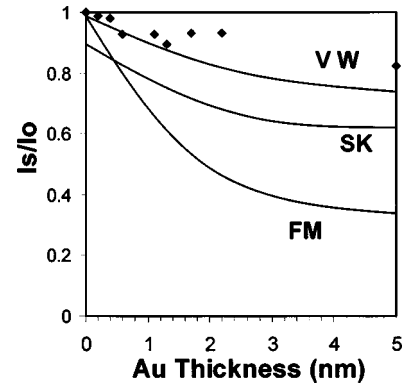


FIG. 5. Attenuation of the O 1s core-level photoelectron peaks as a function of the thickness of a sequentially deposited Au film taken from the XPS spectra (iii)–(x) shown in Fig. 1(a). The experimental data are indicated by solid diamonds for comparison with theoretical curves for Volmer–Weber (VW), Stranski–Krastanov (SK), and Frank–Van der Merwe (FM) thermodynamic growth modes.

The experimental values of I_s/I_o shown in Fig. 5 for the O 1s core level acquired from the cleaned (0001) surface cooled in the plasma ambient decreased from 1.00 before Au deposition to 0.83 ± 0.03 at a nominal Au thickness of 5.0 nm. The I_s/I_o for the Zn 2p_{3/2} for this surface and for the (000 $\bar{1}$) surface followed the same trend. An approximate match to the theoretical curve for VW growth was achieved for deposition on both surfaces. The value of t for each Au deposit was determined using a quartz-crystal deposition rate monitor and, therefore, represents that thickness would be present if the layer was continuous and uniform in thickness across the surface of the ZnO sample. However, as the XPS data (and the TEM results presented below) indicate that the Au nucleated and grew initially as uncoalesced islands, the actual thickness of these islands would have been slightly larger than the value obtained from the rate monitor. Insertion of smaller values of t into Eq. (2) would reduce slightly the values of I_s/I_o and bring the data closer to the theoretical curve for VW growth.

The cross-sectional TEM micrograph in Fig. 6 of an ~ 100 -nm-thick Au film shows (1) the occasional island mi-

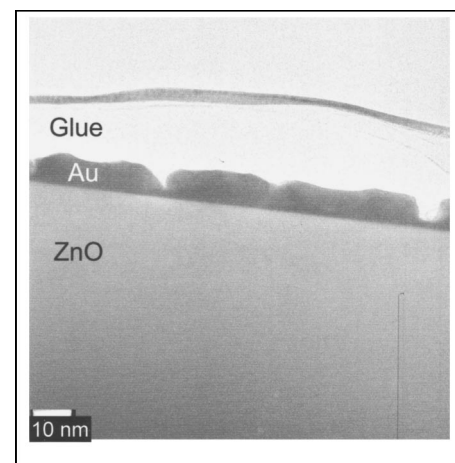


FIG. 6. Cross-sectional TEM images of a Au(111) island and a more common region of coalescence after ~ 100 nm of deposition via electron-beam evaporation.

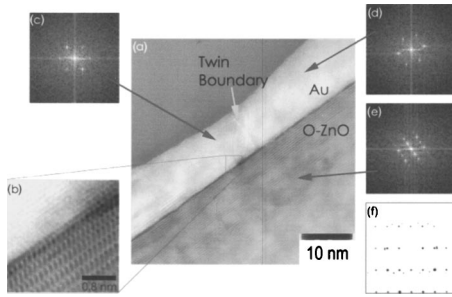


FIG. 7. (a) Moderate and (b) high-resolution TEM images of the plasma-cleaned ZnO(000 $\bar{1}$) wafer/Au film interface. Fast-Fourier transforms (FFT) of gold on (c) the left-hand side and (d) the right-hand side of the twin boundary. (e) FFT of ZnO(000 $\bar{1}$). (f) Superimposed diffraction patterns of ZnO(000 $\bar{1}$) and each side of the twin boundary in the Au film.

crostructure that continued to exist at this thickness, which lends credence to the XPS results regarding the VM mode of growth on a cleaned ZnO(000 $\bar{1}$) surface, and (2) the more common regions of island coalescence. The presence of the glue covering the film indicates that the thickness of the film in this region has not been reduced by ion milling. By contrast, the thickness of one of the areas of coalescence in this film shown in the TEM micrograph in Fig. 7(a) has been reduced to ~ 10 nm during milling. The images in Figs. 7(a) and 7(b) reveal the abrupt clean and unreacted interface between the Au film and the ZnO wafer that are important for Schottky contacts with superior and reproducible electrical characteristics. The diffraction pattern of the interface region produced by the superposition of the patterns obtained from the ZnO and each side of the twin boundary in the Au and shown in Fig. 7(f) proves the epitaxial growth of the Au(111) on the ZnO(000 $\bar{1}$). The double-diffraction spots are due to the twinning of Au, which occurs whenever two islands which nucleate with alternate growth orientations coalesce to produce an incoherent twin boundary. The fast-Fourier transforms (FFTS) acquired on each side of the twinned region and shown in Figs. 7(c) and 7(d) in conjunction with the FFT of the ZnO substrate in Fig. 7(e) correlate with the double-diffraction spots shown in Fig. 7(f).

The curve-fitted XRD spectrum of the Au peak at $38.3^\circ \pm 0.1^\circ$ (FWHM = $0.2^\circ \pm 0.1^\circ$) acquired from the 100-nm-thick Au layer that had been deposited over an entire (0001) surface that had been cleaned and cooled in the plasma ambient is shown in Fig. 8. These results are representative of the XRD spectra acquired from both basal surfaces and reveal that the film is oriented along [111]. The (111) d spacing of 0.0235 ± 0.0001 nm, determined for the film and equivalent to that for single-crystal Au, indicates that this rather thick film had relaxed, i.e., it was no longer coherently strained to match the ZnO surface crystal structure as were the very thin Au films (islands). The XRD results are also in agreement with the results gleaned from the TEM images in that the former indicate that the Au contacts are crystallographically matched to clean ZnO(000 $\bar{1}$) surfaces. It is presumed that these “thick” films also nucleated and grew via the same VM mechanism determined for the sequentially deposited Au films (see above). These results supplement the previous TEM investigations by Wassermann

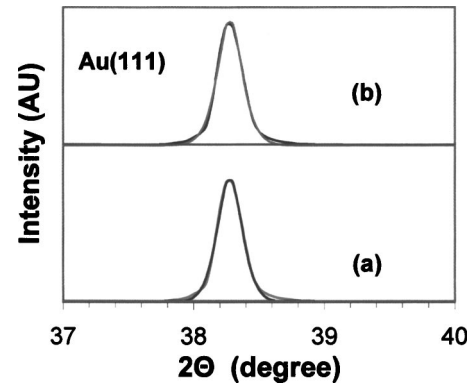


FIG. 8. Curve-fitted XRD 2θ plots obtained from a 100-nm film deposited on a remote plasma-cleaned ZnO(0001) surface cooled in the plasma ambient to room temperature (a) as-deposited and (b) after post-deposition annealing in air at 175°C for 15 min. The spectrum was acquired using Cu $K\alpha$ ($\lambda=0.1542$ nm) radiation.

and Polacek³⁴ that indicated epitaxial growth of Au(111) on the polar surfaces of vacuum-cleaved ZnO. A high degree of structural order was also indicated by the well-defined (1×1) hexagonal LEED pattern with a dark background acquired using an incident energy of 80 eV, from the Au(100nm)/ZnO(000 $\bar{1}$) samples, as shown in Fig. 4(d). The ZnO (0002) and (0004) reflections (not shown) were measured for the lattice at $34.4^\circ \pm 0.1^\circ$ and $72.5^\circ \pm 0.1^\circ$, respectively.

In contrast to the above results, Auger electron spectroscopy (AES) spectra obtained by Roberts and Gorte³⁵ indicated that Pt initially grows in a layer-by-layer mode on a ZnO(0001) surface that has been cleaned via Ar⁺-ion bombardment, annealed in vacuum at 527°C for 30 min, and exposed to 1×10^{-8} Torr of O₂ at 427°C for 30 min. Transmission electron microscopy of the (0001) surface revealed that the Pt(111) plane was parallel to this surface with a 30° rotation between the two lattices. Three-dimensional islands were observed after annealing this sample for an unspecified period at 300°C in vacuum. Henrich and Cox³⁶ have also reported that Pt as well as Pd initially grow by a Frank–van de Merwe mechanism on a ZnO(0001) surface that has been cleaved in vacuum. AES and UPS spectra acquired from polished (0001) surfaces subsequently annealed in UHV confirmed this layer-by-layer growth mode. The [111] directions of the polycrystalline grains of Pd were preferentially oriented parallel to the surface without azimuthal alignment.

D. Determination of the Schottky barrier height from photoemission spectra

The values of Φ_B of the Au/ZnO{0001} interfaces produced in the present research were determined from both XPS and UPS spectra to compare with those values determined from I - V measurements. Fig 1(a) and 1(b) show the respective evolution of the O 1s and the Zn 2p core-level XPS spectra as a function of the thickness of the Au overlayer deposited on cleaned (0001) and (000 $\bar{1}$) surfaces exposed to the plasma ambient on cooling to room temperature. These spectra were acquired *in situ* over an ~ 30 -h period. Deposition of 0.2 nm of Au on the (0001) surface caused the

O 1s lattice peak to shift 0.2 eV from 530.4 to 530.6 eV and the Zn 2p multiplet to shift 0.3 eV from 1021.4 and 1044.5 eV to 1021.7 and 1044.8 eV, respectively. Deposition of an additional 0.2 nm of Au caused the O 1s core level to shift 0.1 to 530.7 eV; the Zn 2p remained unchanged. A similar deposition of 0.2 nm of Au on the (000 $\bar{1}$) surface caused the O 1s lattice peak to shift by 0.5 eV from 530.3 to 530.8 eV, while the Zn 2p_{3/2} and Zn 2p_{1/2} core-level spectra shifted by 0.4 eV from 1021.4 and 1044.5 eV to 1021.8 and 1044.9 eV. Deposition of an additional 0.2 nm of Au did not cause an additional shift in either the O 1s or the Zn 2p core levels. The core-level positions and the intensity and FWHM of the peaks of both the O 1s and the Zn multiplet remained essentially fixed after subsequent depositions on both surfaces to a final thickness of 5.0 nm, indicating that (a) essentially all of the island growth was vertical with only occasional coalescence to this thickness, (b) additional metallization does not affect band bending, and (c) the Schottky barrier is completely formed after the deposition of 0.2–0.4 nm of Au. The agreement in shifts of the O 1s and the Zn 2p core levels for both surfaces provides evidence for the interpretation of the observed shifts as changes in band bending rather than chemically induced shifts.

The evolution of the Au 4f_{7/2} curve-fitted core-level peak during sequential Au depositions on the (0001) and (000 $\bar{1}$) surfaces shown in the XPS spectra in Figs. 9(a) and 9(b), respectively, and in the data presented in Tables I and II, respectively, provided additional information regarding the formation of the Au Schottky barrier. The curve-fitted data are presented to isolate this peak from the Zn 3p_{3/2} and the Zn 3p_{1/2} core-level peaks at 89 and 91 eV, respectively. As noted above, the average actual thickness of the gold islands should be slightly greater than the measured thickness determined from the deposition rate monitor. The results presented in Tables I and II show (i) that the integrated area of the Au 4f_{7/2} peak increased as a function Au thickness, (ii) a significant shift (decrease) in the binding energy (the value of the center of this peak) for Au deposited on the (0001) surface from an initial value of 85.3 eV at 0.2 nm to 84.2 eV for 5 nm of Au ($\Delta=1.1$ eV), (iii) a significant shift in binding energy of this peak for Au deposited on the (000 $\bar{1}$) surface from an initial value of 84.8 eV at 0.2 nm to 84.3 eV for 5 nm of Au ($\Delta=0.5$ eV), and (iv) a significant decrease in the FWHM of these peaks from 2.5 to 1.2 eV ($\Delta=1.3$ eV), as a function of Au thickness on both surfaces.

The following equation³⁷ was used to calculate the value of Φ_B from these results.

$$\Phi_B = E_g - E^f + (E_{\text{core}}^i - E_{\text{VBM}}^i), \quad (4)$$

where E_g is the room-temperature band gap of ZnO (3.4 eV), E^f is the final position of the Zn (or O) core level after 0.4 nm of Au deposition E_{core}^i is the position of the Zn (or O) core level before metal deposition, and E_{VBM}^i is the Fermi-level position relative to the valence-band maximum (VBM) for the cleaned surface cooled in the plasma ambient. The value of E_{VBM}^i was determined from UPS measurements to be 2.8 eV. The value of Φ_B calculated using the data for both the Zn 2p_{3/2} and the O 1s core levels for the (0001) surface

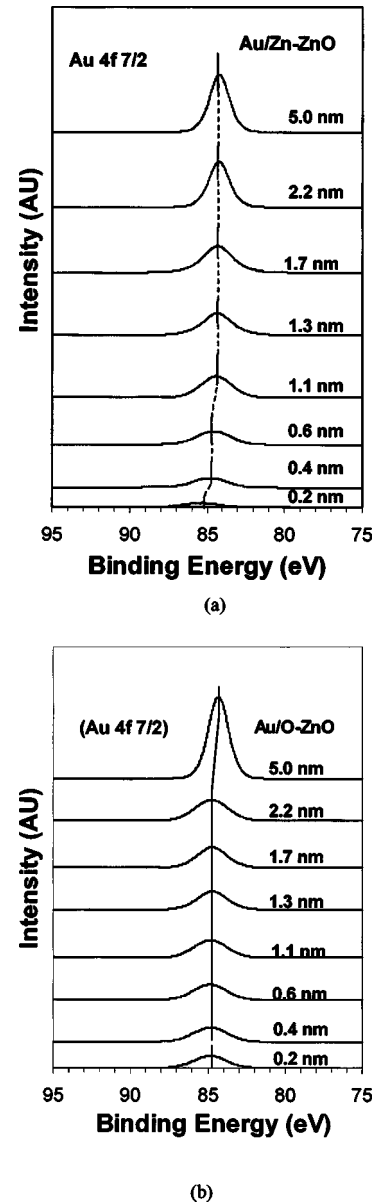


FIG. 9. XPS Au 4f_{7/2} core-level curve-fitted spectra as a function of the sequential deposition of a Au film following remote plasma cleaning and cooling in the plasma ambient on the (a) ZnO(0001) and the (b) ZnO(000 $\bar{1}$) surfaces. All spectra were acquired using Mg K α ($h\nu=1253.6$ eV) radiation.

is 0.3 ± 0.1 eV; the values calculated using the data for these core levels for the (000 $\bar{1}$) surface are 0.2 ± 0.1 and 0.1 ± 0.1 eV, respectively.

The UPS results presented in Fig. 2(a) for the (0001) surface show that the binding energy of the O 2p core level shifted from 4.0 eV for the cleaned surface cooled in the plasma ambient [spectrum (iii)] to 4.4 eV after the deposition of 0.2 nm of Au [spectrum (iv)]. A corresponding shift occurred in the Zn 3d peak from 10.4 to 10.7 eV. The position of the O 2p peak remained unchanged following the next 0.2 nm of Au deposition (0.4-nm total thickness); however, the Zn 3d shifted slightly to 10.8 eV. The Au 5d feature at 6.2 eV also began to emerge at 0.4 nm of growth and increased as a function of Au thickness. The results presented in Fig. 2(b) for the (000 $\bar{1}$) surface show that the binding energy of the O

TABLE I. Au $4f_{7/2}$ core-level data as a function of Au overlayer thickness acquired from the plasma-cleaned ZnO(0001) surface.

Gold $4f_{7/2}$ XPS core-level parameters (± 0.1 eV)			
Experiment step	Integ. area	Center (eV)	FWHM (eV)
Clean/O ₂ adsorbed ZnO(0001)
0.2-nm Au	361	85.3	2.5
0.4-nm Au	390	84.8	2.5
0.6-nm Au	421	84.6	2.5
1.1-nm Au	684	84.4	2.3
1.3-nm Au	697	84.3	2.2
1.7-nm Au	849	84.3	2.2
2.2-nm Au	1456	84.2	1.5
5.0-nm Au	1838	84.2	1.5
100 nm Au (bulk)	...	84.0	1.2
Net shift (eV)	...	1.3	1.3

$2p$ core level shifted from 4.0 eV for the cleaned surface cooled in the plasma ambient [spectrum (iii)] to 4.5 eV, after the deposition of 0.2 nm of Au [spectrum (iv)]. A corresponding shift occurred in the Zn $3d$ peak from 10.4 to 10.8 eV. The large peak in the high binding-energy region of these curves is due to secondary electrons.²¹

The correlation of these peak shifts with those measured by XPS again indicates that the former are caused by the changes in band bending rather than chemical shifts or charging effects. The positions of the peaks of both the O $2p$ and the Zn $3d$ remained essentially fixed after subsequent depositions on both surfaces indicating that (a) additional metallization does not affect band bending and (b) the Schottky barrier is completely formed after the deposition of ~ 0.2 nm of Au, in agreement with the XPS results. In related studies, UPS spectra acquired by Göpel *et al.*³⁸ indicated that Schottky barrier formation occurred over the first 1.0 nm of metal coverage on ZnO(10 $\bar{1}$ 0) without an interface reaction. No surface states were observed in the present research, as also reported by Göpel *et al.*³⁸ Fermi-level pinning was also not observed. The following equation³⁷ was used to calculate the value of Φ_B from these results:

TABLE II. Au $4f_{7/2}$ core-level data as a function of Au overlayer thickness acquired from the plasma-cleaned ZnO(000 $\bar{1}$) surface.

Gold $4f_{7/2}$ XPS core-level parameters (± 0.1 eV)			
Experiment step	Integ. area	Center (eV)	FWHM (eV)
Clean/O ₂ adsorbed ZnO(000 $\bar{1}$)
0.2-nm Au	602	84.8	2.5
0.4-nm Au	730	84.8	2.5
0.6-nm Au	744	84.8	2.5
1.1-nm Au	863	84.8	2.5
1.3-nm Au	898	84.7	2.2
1.7-nm Au	972	84.3	2.2
2.2-nm Au	1035	84.8	2.5
5.0-nm Au	3230	84.3	1.5
100-nm Au (bulk)	...	84.0	1.2
Net shift (eV)	...	0.8	1.3

$$\Phi_B = E_g - E_{\text{VBM}}^f, \quad (5)$$

where E_g is the room-temperature band gap of ZnO (3.4 eV) and E_{VBM}^f (3.2 eV) is the Fermi level relative to the VBM of ZnO for a 0.4-nm Au-coated surface and the Fermi level position. The use of Eq. (5) generated a value for Au on the (0001) surface of $\Phi_B = 0.2 \pm 0.1$ eV, which agrees with the XPS value of 0.3 ± 0.1 eV. For the (000 $\bar{1}$) surface the value of $\Phi_B = 0.1 \pm 0.1$ eV was obtained, which again agrees with the XPS values.

Important information was gleaned from the XPS and UPS studies regarding the occurrence of chemically induced shifts in the spectra, the thickness of Au necessary to form the Schottky barrier, and the microstructure of the Au deposit to a thickness of ~ 5 nm. However, the very low values of Φ_B determined from these photo-optical studies are considered untenable. The emitted spectra may have been compromised, in part, by the presence of Au islands of different effective diameters. However, we believe that the spectra were more strongly affected by the different vertical positions of these very thin islands (or sections within islands) due to the large density of microvoids in the ZnO wafers having different depths from the surface, as discussed more fully at the end of the following section.

E. I - V - T characterization of Au contacts; determination of Φ_B

The I - V data obtained from the Au contacts deposited on grade-I wafers were analyzed using the following methodology. For thermionic emission and V greater than $3 kT/q$, the general diode equation in forward bias is

$$J = J_0 \exp\left(\frac{qV - IR}{nkT}\right), \quad (6)$$

where J is the current density, q is the charge of an electron, V is the voltage, I is the current, R is the series resistance, n is the ideality factor, k is Boltzmann's constant, and T is the absolute temperature. The saturation current density $J_0 = A^* T^2 \exp(-\Phi_B/kT)$ where A^* is the Richardson constant. The theoretical value³⁹ of $A^* = 32 \text{ A cm}^{-2} \text{ K}^{-2}$ was used in this study since the experimental value was not determined. The ideality factors were obtained for Au deposited on the (0001) surface by fitting the forward bias $\ln(J) - V$ curve between 0.22 and 0.29 V for the unheated samples and between 0.08 and 0.23 V for the annealed samples over several decades of current and correcting for the substrate series resistance value obtained by C - V measurements. The ideality factors were similarly obtained for Au deposited on the unheated (000 $\bar{1}$) surface between 0.1 and 0.2 V. Barrier height measurements could not be obtained using C - V measurements due to the high series resistance of the unintentionally doped, 2-mm-thick wafers. Previous results indicated that top-side and bottom-side Ti contacts showed good ohmic behavior through the bulk ZnO wafer. The characteristics of the best Au-rectifying contacts on all sample types are presented and discussed.

I - V measurements at 20 °C of the Au contacts (optically measured contact area = $2.40 \times 10^{-4} \text{ cm}^2$) deposited on *ex situ*

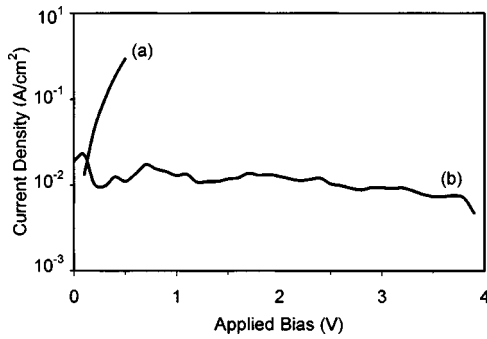


FIG. 10. J - V characteristics in (a) forward and (b) reverse bias of Au contacts deposited on an as-loaded ZnO(000 $\bar{1}$) surface.

cleaned, as-loaded ZnO(000 $\bar{1}$) wafers revealed reverse bias leakage current densities below ~ 0.01 A/cm 2 to 3.75 V reverse bias, as shown in curve (b) in Fig. 10. The ideality factors calculated from this data were >2 , thus making non-sensible any calculated value of Φ_B or J_0 . Soft breakdown began at -3.75 V. These effects are attributed to the presence of the hydroxide on the surface, which forms an accumulation layer which, as noted previously, results in a shallow surface donor character and increases markedly the measured conductivity of the ZnO material. Notable improvements in the I - V characteristics were obtained for the Au contacts (optically measured contact area = 2.40×10^{-4} cm 2) on a plasma-cleaned ZnO(000 $\bar{1}$) surface cooled in the vacuum, as shown in curves (a) and (b) in Fig. 11. The value of the ideality factor was reduced to 1.86 ± 0.05 . Though we recognize that this ideality value is still large and leads to increased uncertainty, we determined a barrier height of 0.67 ± 0.05 eV based on $J_0 = (6 \pm 5) \times 10^{-5}$ A/cm 2 . An $\sim 1.6 \times 10^{-5}$ A/cm 2 leakage current density was measured to 4-V reverse bias with soft breakdown at -4.5 V. The reduction in the hydroxide layer and adventitious carbon generated a 0.7-eV shift in the band bending and the surface Fermi-level position, as shown in Figs. 3(a) and 3(b), which paralleled the enhancement of the rectifying contact properties.

Cooling the cleaned (000 $\bar{1}$) surface in the unignited plasma gas to room temperature and the resulting oxygen adsorption resulted in a lower barrier height of 0.60 ± 0.05 eV, a higher saturation current density of $2.0 \pm 0.5 \times 10^{-4}$ A/cm 2 , a significantly lower value of n

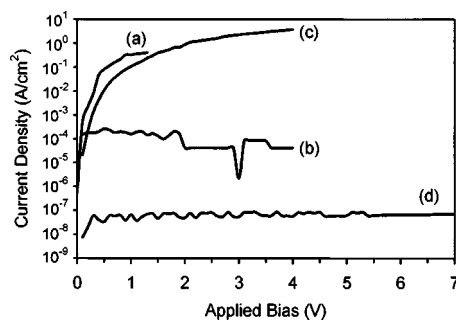


FIG. 11. J - V characteristics of Au contacts deposited on a remote plasma-cleaned ZnO(000 $\bar{1}$) surface cooled in vacuum in (a) forward and (b) reverse bias and for contacts deposited on a similarly cleaned (000 $\bar{1}$) surface and cooled in the plasma ambient in (c) forward and (d) reverse biases.

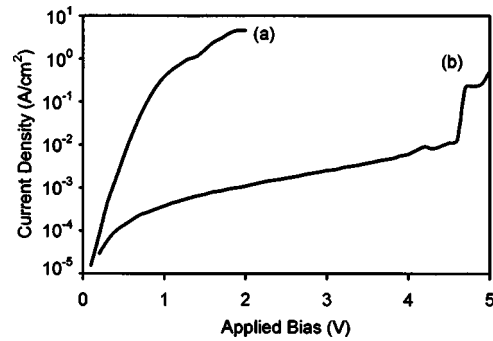


FIG. 12. J - V characteristics of the best Au contacts deposited on an as-loaded ZnO(0001) surface in (a) forward and (b) reverse biases.

$= 1.03 \pm 0.05$, a much lower leakage current of ~ 91 nA/cm 2 to 7 V reverse bias and soft breakdown at this voltage, as shown in curve (d) in Fig. 11. Thirty-three percent of these contacts exhibited leakage currents in the 10–100 nA/cm 2 range compared to 11% of the contacts that were cooled in vacuum from 425 $^{\circ}$ C. Cooling in the plasma ambient generated a 0.5-eV shift in band bending and the surface Fermi-level position, as shown in Figs. 3(b) and 3(c), which enhanced the rectifying properties of these contacts relative to those deposited on this surface [and the (0001) surface] cooled in vacuum. Presumably, the atomically stepped ZnO(000 $\bar{1}$) surface caused the typical amount of 0.2-eV Schottky barrier lowering.⁴⁰

The results of the calculations involving the data obtained from room-temperature (~ 293 K) I - V measurements of the Au contacts on *ex situ* cleaned, as-loaded ZnO(0001) wafers are shown in Fig. 12 for a representative sample. These contacts (optically measured contact area = 2.20×10^{-4} cm 2) had reverse bias leakage current densities below ~ 0.01 A/cm 2 —4.6 V before sharp, permanent breakdown, as shown in curve (b) in this figure. The ideality factors were again >2 . These values and difficulties were again a result of the donor-type surface hydroxide.

Significant improvements in the I - V characteristics in forward and reverse biases were also obtained for the Au contacts (optically measured contact area = 2.20×10^{-4} cm 2) deposited on cleaned ZnO(0001) surfaces cooled in the plasma ambient to room temperature, as shown in curves (a) and (b), respectively, in Fig. 13. These improvements also correspond to the change in electronic band structure shown in Figs. 3(a) and 3(c). This procedure resulted in contacts having a barrier height of 0.71 ± 0.05 eV, a saturation current density of $(4 \pm 0.5) \times 10^{-6}$ A/cm 2 (2.20×10^{-4} cm 2 contact area), a value of $n = 1.17 \pm 0.05$, a significantly lower leakage current density of $\sim 1.0 \times 10^{-4}$ A/cm 2 at -8.5 V reverse bias [curve (b)], and a sharp, permanent breakdown at ~ -8.75 V [curve (b)]. The slightly higher breakdown voltages determined for Au on this surface compared to ~ -7 V for the (000 $\bar{1}$) surface may be associated with a lower barrier height for contacts on the latter surface. Thirty-one percent of these contacts exhibited leakage current densities of the order of 4 μ A/cm 2 at ~ 5 V; the balance of the contacts were influenced by defects, including scratches on the ZnO(0001) surface. As noted in the Introduction, Ra-

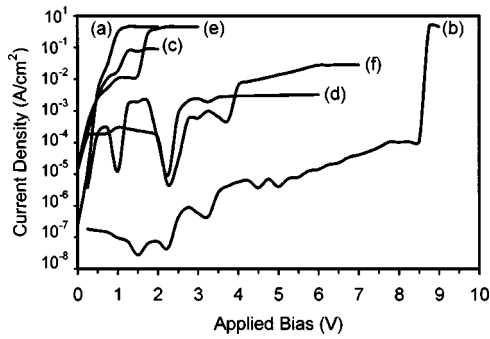


FIG. 13. J - V characteristics of the best Au contacts deposited on a ZnO(0001) surface previously cleaned via remote plasma and cooled in the plasma ambient and determined in forward bias [curves (a), (c), and (e)] and in reverse bias [corresponding curves (b), (d), and (f)] at 20, 80, and 150 °C, respectively.

badanov *et al.*¹² and Neville and Mead¹³ have reported values of the Φ_B of 0.65 and 0.66 eV for Au contacts deposited on UHV-cleaved and chemically prepared surfaces, respectively, of unspecified orientation and in agreement with our calculations from I - V measurements. The measured barrier heights in these three studies, though similar, differ markedly from the predicted Schottky-Mott value of 1.0 eV, even after accounting for potential Schottky barrier lowering, indicating that the interface structure also significantly affects the Schottky barrier. These differences between the theoretical and the measured barrier heights also infer the presence of an interface dipole. However, no significant polarity effects on the rectifying properties were observed between the ZnO(0001) and the ZnO(000 $\bar{1}$) surfaces.

The significantly lower values of the barrier height obtained from our photoemission data relative to those obtained from the I - V data acquired on much thicker films may be due, in part, to the prevalence of Au islands at the nominal metal thickness of 0.4 nm at which the former data were acquired and used in the calculations of Φ_B . Current-voltage measurements using bulk metal contacts are relatively insensitive to the effects that influence photoemission results (e.g., island formation during the initial stages of growth) and, in this case, more likely to give the more accurate values of Φ_B . We believe that the more plausible explanation for the differences in the values of Φ_B is the effect on the photoemission spectra of the microvoids that constituted at least 40% of the ZnO surface, as shown in Fig. 14. The deposition of the Au onto the ZnO surface and to varying depths below the surface during each evaporation would be sufficient to cause core-level shifts as a function of the thickness of the Au layer that, in turn, would influence the values of Φ_B . The optical observation of the contacts to be used for the I - V measurements was an important step, as some of the voids extended through the bulk of the substrate and others were joined together to make a larger void and pinholes in the contacts. These extended defects (and associated contacts) were avoided in the I - V measurements; however, they very likely influenced the photoemission data.

The contacts deposited on the (0001) surface were also heated to 80 ± 5 and 150 ± 5 °C and the electrical properties determined at these annealing temperatures, as shown in

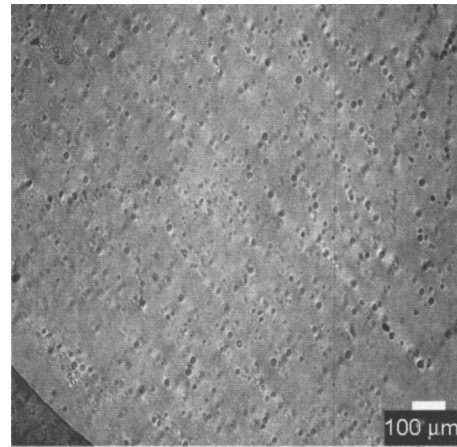


FIG. 14. Optical micrograph of ZnO(000 $\bar{1}$) surface showing numerous voids that extended various lengths into the wafer.

curves (c)–(f) in Fig. 13. The I - V - T measurements at 80 °C showed an increase in the barrier height to 0.82 ± 0.05 eV, a higher saturation current density of $9.05 \mu\text{A}/\text{cm}^2$, a decrease in the value of n to 1.12 ± 0.05 , and an increase in the leakage current density to $\sim 2 \text{ mA}/\text{cm}^2$ at 6 V reverse bias [curve (d)]. Breakdown measurements were not taken for the data displayed in curve (d). Further reduction in the reverse bias performance was detected in the sample heated to 150 °C, as shown in curve (f). A barrier height of 0.79 ± 0.05 eV, a saturation current density of $4.34 \mu\text{A}/\text{cm}^2$, a lower value of $n = 1.09 \pm 0.05$, a leakage current density of $\sim 20 \text{ mA}/\text{cm}^2$ to 7.0 V reverse bias, and a soft, permanent breakdown at this voltage were determined from these results. Thermal cycling of the contacts between the two annealing temperatures and room temperature had no measurable impact on the rectifying properties. The relocation of the thermally generated carriers in shallow electron traps is likely the mechanism causing the increased reverse bias leakage current as the temperature is increased. Slight changes in the interface structure and/or chemistry during the I - V - T measurement may explain the small variance in n and Φ_B .

IV. SUMMARY

Unpatterned Au films deposited *in situ* on n -type ZnO(0001) and ZnO(000 $\bar{1}$) wafers previously cleaned using a 20% O₂/80% He remote plasma at 550 and 525 °C, respectively, and cooled in the unignited plasma ambient, nucleated and initially grew via the Volmer-Weber (island) mode. It is presumed that the similarly deposited Au Schottky contacts initially grew via the same mechanism. Calculations using the I - V results obtained from the best contacts deposited on the *ex situ* cleaned, as-loaded (0001) [(000 $\bar{1}$)] surfaces revealed a reverse bias current density of ~ 0.01 (~ 0.1) A/cm² to 4.6 (3.75) V and ideality factors of $n > 2$ for both surfaces before sharp, permanent breakdown (soft breakdown) occurred. These results were ascribed to the presence of $(1.6\text{--}2.0) \pm 0.1$ [(0.7–2.6) ± 0.1] ML of hydroxide, which typically increases the surface conductivity via the formation of an accumulation layer. The results of XPS and UPS studies showed that plasma cleaning and cool-

ing both surfaces in vacuum eliminated all detectable hydrocarbon contamination, reduced the amount of the hydroxide layer to ~ 0.4 ML, and resulted in a 0.7-eV reduction in downward band bending and a 0.7 eV lowering of the surface Fermi level. The surfaces of the cleaned wafers were also smooth, highly ordered, and stoichiometric. Cooling in the plasma ambient caused the chemisorption of oxygen and a change from 0.2 eV of downward band bending to 0.3 eV of upward band bending, indicative of a depletion layer and lower surface conductivity. The best gold contacts measured on the (0001) [(0001) $\bar{1}$] surfaces possessed a barrier height of 0.71 ± 0.05 (0.60 ± 0.05) eV, a saturation current density of $4 \pm 0.5 \times 10^{-6}$ A/cm² [$(2.0 \pm 0.5) \times 10^{-4}$ A/cm²], a lower value of $n = 1.17 \pm 0.05$ (1.03 ± 0.05), and a significantly lower leakage current density of $\sim 1.0 \times 10^{-4}$ A/cm² ($\sim 91 \times 10^{-9}$ A/cm²) at 8.5 (7.0) V reverse bias prior to sharp, permanent breakdown (soft breakdown). The lower values of Φ_B calculated from the photoemission data relative to those obtained from the I - V data acquired on much thicker films may have been influenced by the presence of Au islands. However, the more likely cause of the lower values of Φ_B was the presence of microvoids of various depths in the surface of substrates which allowed the very thin Au islands to be deposited at various depths which, in turn, influenced the photoemission spectra. All measured barrier heights were lower than the predicted Schottky-Mott value of 1.0 eV. It has recently been shown that the Schottky barrier can be described in terms of the interface dipole that develops due to the bonding at the interface.⁴¹ The results presented here support this model and may provide a basis for describing the interface dipole at the metal-ZnO interface. Defects at the Au/ZnO(0001) interface structure are the likely cause of this difference. Constancy of the FWHM of core levels for Zn 2p (1.9 eV) and O 1s (1.5 eV), before and after sequential Au depositions conducted, *in situ* indicated an atomically abrupt, unreacted Au/ZnO(0001) interface which was confirmed via TEM studies. Data acquired at temperature during annealing of the contacts on the (0001) surface to 80 ± 5 and 150 ± 5 °C revealed decreases in the ideality factors to 1.12 ± 0.05 and 1.09 ± 0.05 and increases in saturation current density to 9.05 and $4.34 \mu\text{A}/\text{cm}^2$, the barrier height to 0.82 ± 0.5 and 0.79 ± 0.5 eV, and in the leakage current densities to $\sim 2 \times 10^{-3}$ A/cm² at -6 V and $\sim 20 \times 10^{-3}$ A/cm² at -7 V, respectively. These values were not affected by repeated cycling between room temperature and the elevated temperature of choice. The [111] crystallographic orientation of the contacts was unchanged during heating. We do not know the precise reason(s) for the improvements in the electrical character of the contacts after heating; however, it may be that the annealing improved slightly the epitaxial relationship between the two materials.

ACKNOWLEDGMENTS

This research was partially funded by both the Kenan Institute for Technology, Engineering and Science at North Carolina State University, and by the Office of Naval Research under Contract No. N00014-98-1-0654 (H. Dietrich, monitor). One of the authors (R.F.D.) was partially supported by a Kobe Steel Ltd. Professorship. The authors acknowl-

edge their appreciation to Professor Gerry Lucovsky of NCSU for the use of C - V equipment and to Zach Reitmeier and Seann Bishop for assistance with the figures.

- ¹D. C. Look, *Mater. Sci. Eng., B* **80**, 383 (2001).
- ²S. J. Pearton, D. P. Norton, K. Ip, Y. W. Heo, and T. Steiner, *Superlattices Microstruct.* **34**, 3 (2003).
- ³P. Bonasewicz, W. Hirschwald, and G. Neumann, *Appl. Surf. Sci.* **28**, 135 (1987).
- ⁴A. F. Kohan, G. Ceder, D. Morgan and C. G. Van de Walle, *Phys. Rev. B* **61**, 15019 (2000).
- ⁵C. G. Van de Walle, *Phys. Rev. Lett.* **85**, 1012 (2000).
- ⁶N. Y. Garces, N. C. Giles, L. E. Halliburton, G. Cantwell, D. B. Eason, D. C. Reynolds, and D. C. Look, *Appl. Phys. Lett.* **80**, 1334 (2002); (private communication).
- ⁷H. Fabricius, T. Skettrup, and P. Bisgaard, *Appl. Opt.* **25**, 2764 (1986).
- ⁸F. D. Auret, S. A. Goodman, M. Hayes, M. J. Legodi, H. A. van Laarhoven, and D. C. Look, *Appl. Phys. Lett.* **79**, 3074 (2001).
- ⁹F. D. Auret, S. A. Goodman, M. Hayes, M. J. Legodi, W. E. Meyer, and D. C. Look, *Appl. Phys. Lett.* **80**, 1340 (2002).
- ¹⁰Y. Kanai, *Jpn. J. Appl. Phys., Part 1* **29**, 1426 (1990).
- ¹¹N. F. Mott, *Proc. Cambridge Philos. Soc.* **34**, 568 (1938).
- ¹²R. A. Rabadanov, M. K. Guseikhanov, I. Sh. Aliev, and S. A. Semiletov, *Fizika (Zagreb)* **6**, 72 (1981).
- ¹³R. C. Neville and C. A. Mead, *J. Appl. Phys.* **41**, 3795 (1970).
- ¹⁴N. Ohashi, J. Tanaka, T. Ohgaki, H. Haneda, M. Ozawa, and T. Tsurumi, *J. Mater. Res.* **17**, 1529 (2002).
- ¹⁵Y. Liu, C. R. Gorla, S. Liang, N. Emanetoglu, Y. Lu, H. Shen, and M. Wraback, *J. Electron. Mater.* **29**, 69 (2000).
- ¹⁶H. Sheng, S. Muthukumar, N. W. Emanetoglu, and Y. Lu, *Appl. Phys. Lett.* **80**, 2132 (2002).
- ¹⁷A. Y. Polyakov, N. B. Smirnov, E. A. Kozhukhova, V. I. Vdovin, K. Ip, Y. W. Heo, D. P. Norton, and S. J. Pearton, *Appl. Phys. Lett.* **83**, 1575 (2003).
- ¹⁸H. von Wenckstern *et al.*, *Appl. Phys. Lett.* **84**, 79 (2004).
- ¹⁹B. J. Coppa, R. F. Davis, and R. J. Nemanich, *Appl. Phys. Lett.* **82**, 400 (2003).
- ²⁰V. E. Henrich and P. A. Cox, *The Surface Science of Metal Oxides* (Cambridge University Press, Cambridge, 1994), p. 297.
- ²¹H. Moormann, D. Kohl, and G. Heiland, *Surf. Sci.* **100**, 302 (1980).
- ²²G. Heiland and P. Kunstmann, *Surf. Sci.* **13**, 72 (1969).
- ²³M. Nakagawa and H. Mitsudo, *Surf. Sci.* **175**, 157 (1986).
- ²⁴E. Arijis, F. Cardon, and W. Maenhout-Van Der Vorst, *Surf. Sci.* **17**, 387 (1969).
- ²⁵L. Lagowski, E. S. Sproles, Jr., and H. C. Gatos, *J. Appl. Phys.* **48**, 3566 (1977).
- ²⁶V. E. Henrich and P. A. Cox, *The Surface Science of Metal Oxides* (Cambridge University, Cambridge, 1994), p. 288.
- ²⁷J. van der Weide, Ph.D. dissertation, North Carolina State University, Raleigh, NC, 1994.
- ²⁸B. J. Coppa, C. C. Fulton, P. J. Hartlieb, R. F. Davis, B. J. Rodriguez, B. J. Shields, and R. J. Nemanich, *J. Appl. Phys.* **95**, 5856 (2004).
- ²⁹S. M. Kiesel, M. S. dissertation, North Carolina State University, Raleigh, NC, 2004.
- ³⁰K. Jacobi, G. Zwicker, and A. Gutmann, *Surf. Sci.* **141**, 109 (1984).
- ³¹V. E. Henrich and P. A. Cox, *The Surface Science of Metal Oxides* (Cambridge University, Cambridge, 1994), p.p. 298–299.
- ³²Z. Sitar, L. L. Smith, and R. F. Davis, *J. Cryst. Growth* **141**, 11 (1994).
- ³³S. D. Wolter, J. M. Delucca, S. E. Mohny, R. S. Kern, and C. P. Kuo, *Thin Solid Films* **371**, 153 (2000).
- ³⁴E. F. Wassermann and K. Polacek, *Appl. Phys. Lett.* **16**, 259 (1970).
- ³⁵S. Roberts and R. J. Gorte, *J. Chem. Phys.* **93**, 5337 (1990).
- ³⁶V. E. Henrich and P. A. Cox, *The Surface Science of Metal Oxides* (Cambridge University, Cambridge, 1994), pp. 396–97.
- ³⁷K. M. Tracy, Ph.D. dissertation, N. C. State University, Raleigh, NC (2000).
- ³⁸W. Göpel, L. J. Brillson, and C. F. Brucker, *J. Vac. Sci. Technol.* **17**, 894 (1980).
- ³⁹S. M. Sze, *Physics of Semiconductors Devices* (Wiley, New York, 1981), p. 849.
- ⁴⁰J. F. Luy and P. Russer, *Silicon-Based Millimeter-Wave Devices* (Springer, Berlin, 1994), p. 120.
- ⁴¹R. T. Tung, *Phys. Rev. B* **64**, 205310 (2001).